Global aridity synthesis for the last 60 000 years

Florian Fuhrmann[1], Benedikt Diensberg[1], Xun Gong[2], Gerrit Lohmann[2], Frank Sirocko[1]

[1]Department for Geoscience, Johannes-Gutenberg-Universität, Mainz, 55099, Germany

[2]Alfred Wegener Institute for Polar and Marine Research, Bremerhaven, Germany

5   *Correspondence to*: Florian Fuhrmann, (flfuhrma@uni-mainz.de)

Abstract. A compilation of published literature on the dust content in terrestrial and marine sediment cores are synchronised on the basis of pollen data and speleothem growth phases within GICC05 age constrain. Based on that, aridity patterns for ten key areas in the global climate system are reconstructed over the past 60 000 years. These records have different time resolutions and rely on different dating methods, thus of various types of stratigraphy. Nevertheless, all regions show humid
10   conditions during the early MIS3 and early Holocene, but not always of the same timing. Such discrepancies have been interpreted as regional effects while also due to stratigraphical uncertainties. In comparison, the MIS2 interval becomes arid in all northern hemisphere records, but the peak arid conditions of the Last Glacial Maximum (LGM) differ in duration and intensity among regions. In addition, we also make comparisons between the aridity synthesis to modelling results using a Global Climate Model (GCM). Indeed, both lines of evidence show great agreement for the Holocene, LGM and for the late
15   MIS intervals.

1 Introduction

Paleoclimate research today has two focus: i) well dated, high resolution archives of past climate (e.g., marine and terrestrial sediments, speleothems, tree rings and ice cores), ii) modelling of global and regional characteristics with Global Climate Models (GCM), which include main processes in atmosphere, ocean, land and cryosphere as well as their couplings.

20   Accordingly, it is the strength of the geo-archives to provide a view of the precise past of climate and annual-/decadal-/century-/millennial-scale regional evolutions. The strength of modelling approach, on the other hand, is to understand the processes of climate change and its global patterns. The fundamental structure and cause of climate change will be better understood if the results from both lines indeed agree.

This is achieved to a large extent for the Holocene, i.e. Marine Isotope Stage (MIS) 1, 0 - 11 700 years before 2000 CE (yr

25   b2k) and the last deglaciation (14 700 – 11 700 yr b2k), but mechanisms operating during the MIS2 (Last Glacial Maximum (LGM) 24 000-14 700 yr b2k) or the flickering climate of MIS3 (60 000 – 24 000 yr b2k) are not fully understood. The still open mechanistic question is associated with the stability of the large continental ice sheets, which control at least the climate of the high latitudes, but are apparently also teleconnected with global Sea levels (Bintanja and van de Wal, 2008).

In this paper, we evaluate published paleoclimate reconstructions for one of the most important indicators of climate change, which is aridity. We have screened about 2000 papers of the paleoclimate literature of the last 30 years to detect 10 key areas, for which enough information from various lines of evidence is available to bring the information about past aridity to a synthesis. We define these key areas by the proxy availability, i.e. pollen, dust and speleothem growth must provide three

5   independent sources of information related to past precipitation. Many important records of paleoclimatic research are thus not included in these 10 key regions, because only one or two of the aridity proxies are available.

Dust is deflated only in regions with less than 200 mm/a precipitation, and thus indicate a desert climate (either subtropical or polar) (Pye, 1987) Speleothem growth needs dripping water in a cave, and thus rain or snow melt (Spötl and Mangini, 2002). Arboreal pollen implies more precipitation than in a landscape with abundant grass pollen. Accordingly, we do not

10   evaluate the full width of information from these paleoclimate proxies, but just reduce the evidence to its basic structure, which is aridity. The most faithful aridity indicator is dust, which indicates deserts, whereas grass indicates steppic landscapes.

We present the 10 key regions and their basic climate structure during the last 60 000 years (Fig. 1, Fig. 3, Fig. 4). The detailed evidence for each of the 10 key regions and their well dated and high-resolution proxy records are presented in

15   Fig. 2 and Supplement S1-S9. The discussion compares the synoptic aridity reconstruction for the time of LGM and late MIS3 (Fig. 4) with GCM simulations (Fig. 7).
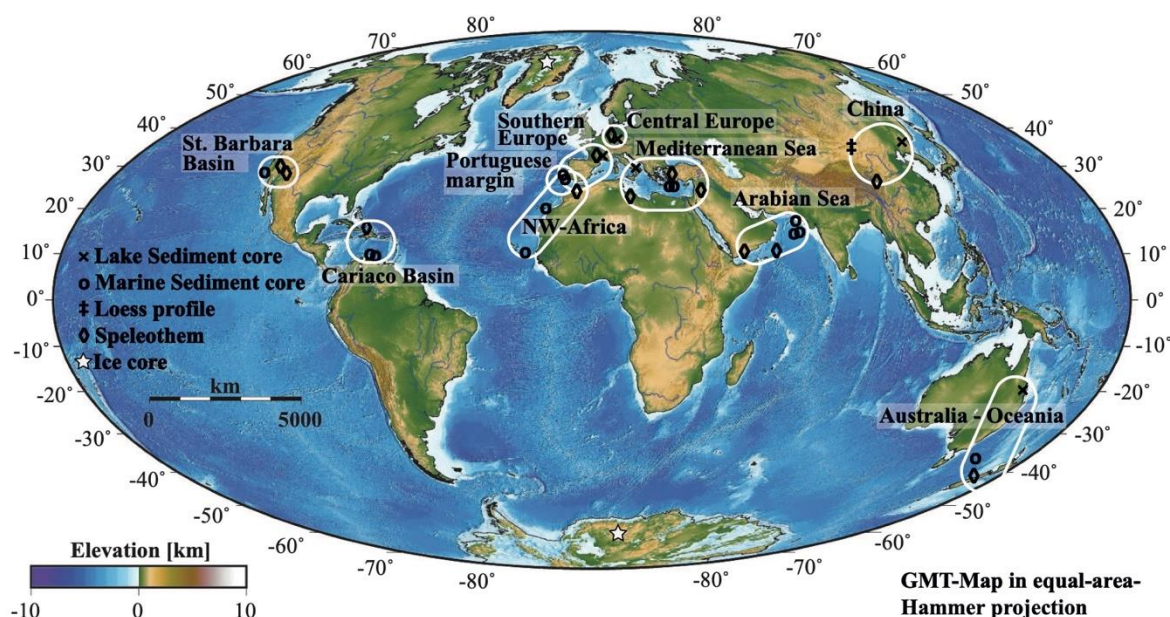
Figure 1: Global map with the 10 key regions and archive type, Generic Mapping Tool (GMT) (Wessel and Smith, 1991). Regions are shown with white boundaries. Crosses sign lake sediment cores; open circles marine sediment cores; double sharp marks loess profile;

20   Diamonds mark speleothems and white stars ice cores. In addition, the map is colour coded for the elevation.

We start the synthesis with our own dust and pollen records from Eifel (Seelos et al., 2009; Sirocko et al., 2016), which we compare with speleothem data from nearby Bunker Cave (Fohlmeister et al., 2012, 2013; Weber et al., 2018) as well as the Spannagel Cave in Austria (Holzkämper et al., 2004; Spötl and Mangini, 2002). The maar sediment cores of the Eifel Laminated Sediment Archive (ELSA)-project (Sirocko, 2016; Sirocko et al., 2016) show all Greenland Stadials (GS) and

5 Interstadials (GI) in the time series of eolian dust content (Dietrich and Sirocko, 2011; Seelos et al., 2009). Central Europe shows accordingly the same climatic structures, which is well known in North Atlantic marine sediments (Hodell et al., 2013; McManus et al., 1994; Naafs et al., 2013) and Greenland ice cores (North Greenland Ice Core Project Members et al., 2004; Rasmussen et al., 2014; Svensson et al., 2008). This North Atlantic – Central European climate time series is then compared with the respective time series from all other 9 key regions, which data evidence is documented in the

10 Supplement.

2 Methods

The comparison is based on pollen profiles from sediment cores, growth phases of speleothems and dust proxies like grain size of eolian fraction within sediment cores. Also, isotope data like δ^{18}O, Sea Surface Temperature (SST) reconstructions or Ice Raft Debris (IRD) data are added to complete the picture. We use the original stratigraphy of all records, but bring them

15 to the GICC05 time scale using the b2k notation.

Speleothems are used for synchronisation between different archives of one region. Especially the growth phases of speleothems are a significant indicator for presence of mobile water or in other words: if a speleothem could grow, at least some precipitation occurred over the cave. If a speleothem does not grow (hiatus), either no precipitation or a change of the drip water system above the cave could be possible causes. Also, the sample frequency plays an important role. The age-

20 errors of speleothem growth data we used for this synthesis, all are below 4 % in total. Some speleothem datasets also provide δ^{18}O isotope measurements, which are interpreted by the original authors as precipitation or temperature signals recorded in the speleothem archive e.g. Genty et al., 2003; Hoffmann et al., 2016; Wainer et al., 2009.

Pollen are separated in two classes for this work. Trees and shrubs (in following only tree pollen) were combined as they require similar climate conditions for their growth. Herbs and grasses (in following only grass pollen) were also combined.

25 Trees need a significantly larger amount of precipitation than grasses to grow. So, a simple statement about the relative precipitation of the catchment area of the core can be done by looking at the tree / grass pollen ratios. In general, a higher amount of tree pollen indicates warmer and wetter climate than high amounts of grass pollen. The time resolution of the pollen profiles is often low, but we have chosen the accessible highest resolution data for the comparison, and the record must have been reliably dated.

30 IRD layers consist of coarse-grained dropstones from iceberg discharge and low foraminifer contents (Heinrich, 1988). They were climatically interpreted as extreme cooling of the SSTs before Greenland interstadials (Bond et al., 1998).

The global climate structure is well documented within Greenland and Antarctica ice cores (Andersen et al., 2006; EPICA community members, 2004; Grootes et al., 1993; North Greenland Ice Core Project Members et al., 2004; Rasmussen et al., 2006; Svensson et al., 2008; WAIS Divide Project Members et al., 2015) and others. The best chronology is from the annual layer counted NGRIP ice core in Greenland (Rasmussen et al., 2014). For northern hemisphere, those ice core data do

5   include not only chemical compositions and isotopes, but also dust. (Ruth et al., 2003, 2007)).

Several dust proxies are used for this synthesis due to a large variety in dust over the several regions. Calcium carbonate ($CaCO_3$) in Portuguese margin, France and Arabian Sea is deposited in higher rates with warmer temperatures (Leuschner and Sirocko, 2003). Larger grains can be deflated only with lower temperatures and higher wind speeds in comparison with strong aridity cases, see grainsize record from Loess Plateau, China (Sun et al., 2010; Xiao et al., 1995, 2015). Dust or eolian

10 content is displayed in percentages of the whole sample composition (Australia - Oceania, NW-Africa). In sediments from the Cariaco Basin, the Al/Ti ratio gives the proportion between terrigenous river sediments with higher Al/Ti ratios and Saharan dust with respective lower Al/Ti ratios (Yarincik et al., 2000). Kaolinite/chlorite (K/C) ratio shows more dust for higher ratio values, due to more kaolinite within the dust than chlorite for Mediterranean Sea region. While humid periods stored the kaolinite within lakes or basins, deflation occurred during arid periods (Ehrmann et al., 2017).

15 **2.1 Aridity index calculation**

Our aridity index is a combined estimate from all available precipitation reconstruction sources showing the dryness of a region over time. Speleothem growth, the amount of tree pollen and dust values are analysed in details. For each dataset, the original values have been recalculated into percentages, proportional to the maximum value of each specific dataset if the original data were not. The tree pollen and eolian dust data are divided in three parts (Tab. 1), speleothems only account for

20 growth or no growth. Dust is considered inverse to tree pollen (higher dust values get lower index values), as lower precipitation and therefore soil humidity are required for dust deflation. Speleothem growth phases, higher tree pollen values and lower dust values combined therefore indicate more humidity and precipitation.

Speleothems		Tree pollen		Eolian dust	
0	no speleothem growth	0	tree pollen values < 33%	0	dust values > 66%
1	speleothem growth	1	tree pollen values > 33% & < 66%	1	dust values < 66% & > 33%
		2	tree pollen values > 66%	2	dust values < 33%

Table 1. Components of the aridity index: Speleothems can either account as value 0 (no speleothem growth) or 1 (speleothem growth);
25 Tree pollen values below 33 % do not add to the aridity index, between 33 % and 66 % they account for 1 and above 66 % for 2; Dust values were internally normalized and act inverse to tree pollen. Dust values above 66 % do not increase the index, between 66 % and 33 % they count as value 1 and below 33 % as value 2. The aridity index ranges from 0 (highly arid conditions) to 5 (highly humid conditions).

2.2 Error estimates

In absence of absolute error indications for most of the used datasets, we applied a simulation based on error estimates to get an approximation of the errors. For this we used the error values as displayed in Tab. 2. Speleothem age errors are calculated from the age uncertainties while pollen and dust errors are estimated.

5 We randomly disturbed the original data with a probability given by the error estimates and calculated a disturbed aridity index from the disturbed data as described in Tab. 1 and chapter 2.1. The variance over 100 000 runs gives the approximate error of our aridity index. This error simulation is based on Koehler et al. (2009).

The so generated error estimations are displayed in Fig. 2 and Figs. S1-S9 by grey colour shades behind the mean data (with 200 year running average) of the aridity index.

Regions	Speleothem age uncertainty [%]	Tree pollen uncertainty [%]	Eolian dust uncertainty [%]
Central Europe	2.66	3	5
Arabian Sea	1.5	1	3
China	2	2	2
NW-Africa	1	10	2
Southern Europe	1	4	2
Portuguese Margin	1	3	2
Cariaco Basin	4	3	2
Mediterranean Sea	2.5	2	3
St. Barbara Basin	1	3	no dust source
Australia - Oceania	4	3	3

Table 2. Error estimations as input to simulation for all 10 key regions for speleothems, tree pollen and eolian dust.

3 Results

3.1 Central European climate for the last 60 000 years

Central Europe is one of the large feedback regions to North Atlantic climate changes. The Atlantic meridional overturning

15 circulation (AMOC) and thus temperature and precipitation strongly influence the whole European continent. Nowadays, the annual mean temperature in Germany is about 9.6 °C and precipitation of about 800 mm/year (Deutscher Wetterdienst, 2018). The Eifel volcanic field in western Germany consists of about 70 maar lakes and dry maar lakes (Büchel, 1994). The maar lakes had a very steep slope resulting in large water volumes and good, anoxic, preservation conditions (Negendank, 1989). Large parts of the cores are warved or at least laminated, which leads to a better understanding of sedimentation

20 processes and results in a good stratigraphy with annual warve counting until 30 000 yr b2k (Sirocko et al., 2016). The LGM and stadial climate were dominated by dusty storms (Schaber and Sirocko, 2005), see Fig. 2. The dust index (Dietrich and Seelos, 2010; Dietrich and Sirocko, 2011; Seelos et al., 2009) reveals the GIs in details. The closest known and well dated speleothems to the Eifel region are from the Bunker Cave in Sauerland (Fohlmeister et al., 2012; Weber et al., 2018) which can be compared to the Spannagel Cave system from western Zillertal, Austria (Holzkämper et al., 2004).

The timespan from 60 000 to 48 000 yr b2k (early MIS3, GIs 17-13) is characterized by a high precipitation visible in the fast speleothem growth of Bunker and Spannagel cave. Nearly 100 % of tree pollen combined with lowest grass and herb pollen values also indicate a strong precipitation amount during that time as well as relatively high temperatures close to present day ones (Sirocko et al., 2016). An intermediate dust content in the ELSA-Dust-Stack and a low dust concentration

5 in the NGRIP ice core suggest an intermediate to low aridity. The change in $\delta^{18}O$ at the begin of GI12 occurred at 46 860 yr b2k (Rasmussen et al., 2014). The pollen composition change began at 49 000 yr b2k towards more grass and herbs pollen. With the begin of Heinrich event 5 (HE5), the dust amount spikes in the ELSA-Dust-Stack as well as in the NGRIP core indicating a strong pulse of aridification at 48 000 yr b2k, ending the humid phase of early MIS3.

The period from 48 000 until 38 500 yr b2k comprises GIs 12-9. The speleothem growth in Spannagel ended before and at

10 45 700 yr b2k, Bunker Cave speleothem growth also stopped after a Hiatus between 50 000 and 46 000 yr b2k and a short growth recovery. The tree pollen decreased to about 50 to 60 %, still more tree pollen than grass pollen, but a considerably lower amount than in early MIS3. While the dust amount in the ELSA-Dust-Stack rises to higher intermediate values, the pattern within the NGRIP is characterized by the stadial pulses. ELSA-Dust-Stack, NGRIP dust and NGRIP $\delta^{18}O$ show the same pattern and react apparently on the same overlaying mechanism.

15 From 38 500 to 22 000 yr b2k (GIs 8-2) a change towards lower precipitation and higher aridity occurred. No speleothem growth is documented from Bunker or Spannagel cave. The pollen concentration shows higher grass and herbs content and lower tree pollen percentages, but still some birch and pine trees were present during this time (Sirocko et al., 2016). The ELSA-Dust-Stack comprises of multiple changes within this timespan and shows the general dust content as relatively high with larger variability. The NGRIP in contrast shows the highest dust concentrations in the time between 23 000 and

20 26 000 yr b2k, a phase where the dust content in the ELSA-Dust-Stack is high, but not at maximum values. The NGRIP $\delta^{18}O$ whereas shows a long phase of extreme cold temperatures during this phase (Kindler et al., 2014).

The timespan of 22 000 to 14 300 yr b2k also does show no speleothem growth as well as a complete absence of pollen. The precipitation was at the lowest values of the whole record, while the ELSA-Dust-Stack shows the highest dust amounts from 23 000 up to 15 000 yr b2k. The NGRIP dust concentrations are however on intermediate values during that time suggesting

25 a different transport and sedimentation regime between these two regions in the time from 26 000 to 15 000 yr b2k. With the end of the large dust dominated LGM at 15 000 yr b2k, the revival of vegetation followed shortly after 14 300 yr b2k (Litt and Stebich, 1999). Younger Dryas (YD) is apparent in the pollen data by a grass pollen increase and the last deglaciation is marked by a sharp increase in tree pollen. Throughout the Holocene, tree pollen values range around 90 %. The dust content of the ELSA-Dust-Stack varies between intermediate to low levels. Speleothem growth started again at 11 197 (± 94) yr b2k

30 and continues through the whole Holocene. Also, the $\delta^{18}O$ of the NGRIP shows constant high values with exception of the YD event. The time from 14 300 yr b2k up to present day can be described as a humid phase with intermediate to high precipitation and moderate temperatures.
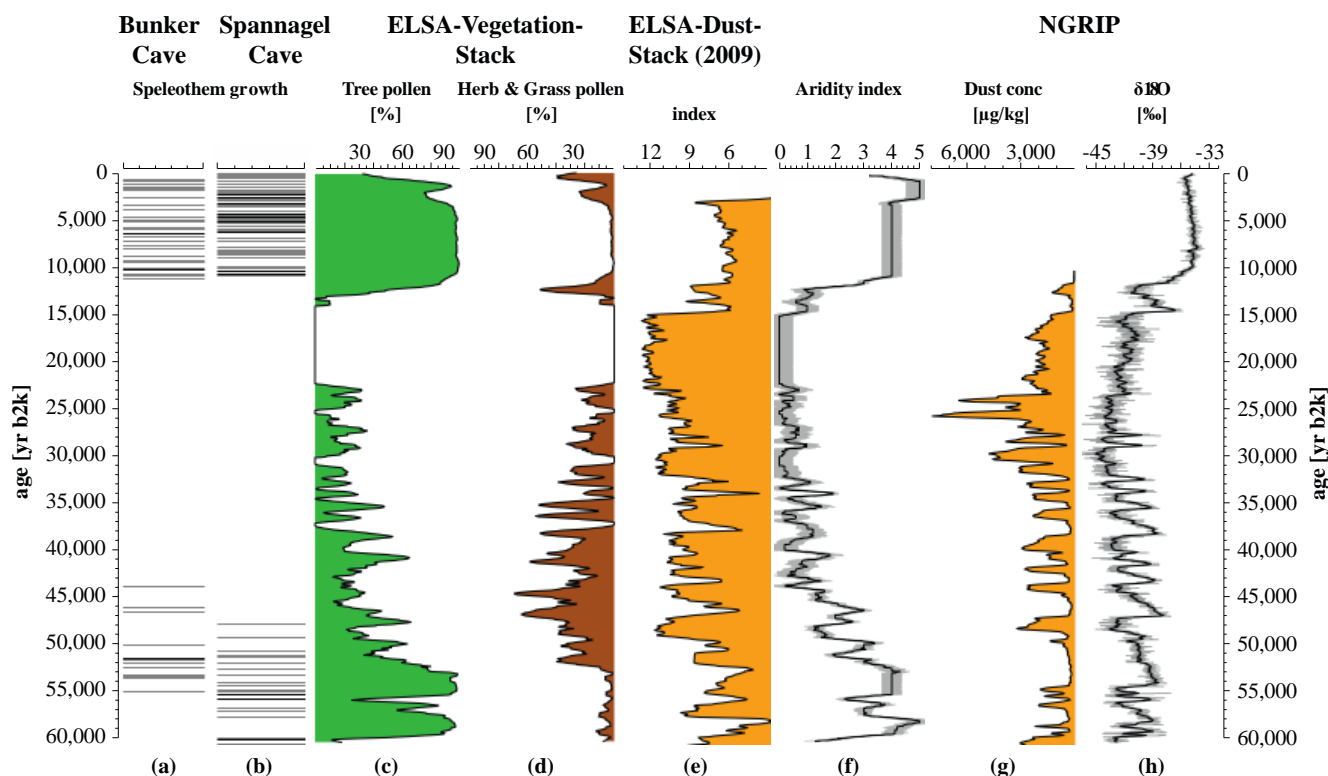
Figure 2: Central European climate over the last 60 000 years: **(a)** Bunker Cave (Fohlmeister et al., 2012, 2013; Weber et al., 2018) and **(b)** Spannagel Cave (Holzkämper et al., 2004; Spötl and Mangini, 2002) show speleothem growth phases, which require mobile water from frequent precipitation; **(c, d)** ELSA-Vegetation-Stack pollen data (Sirocko et al., 2016) are divided into tree- and herb & grass pollen. While trees require more precipitation, grasses are dominant for more arid conditions; **(e)** ELSA-Dust-Stack (Seelos et al., 2009) indicates more arid conditions with higher values, lower values account for more humid conditions. GIs are distinguishable by lower index values and are highly comparable to **(h)**; **(f)** Aridity index for Central Europe as result from **(a-e)**, for detailed information see method section; **(g)** Dust concentration from NGRIP ice core (Ruth et al., 2007); **(h)** δ^{18}O data from NGRIP ice core (North Greenland Ice Core Project Members et al., 2004) in comparison.

The Central Europe region acts not only as an example, but as reference for the other regions due to its comparability to the North Atlantic and Greenlandic ice cores. For further detailed information on the other nine regions see Supplement S1-S9.

3.2 Aridity reconstruction of the last 60 000 years
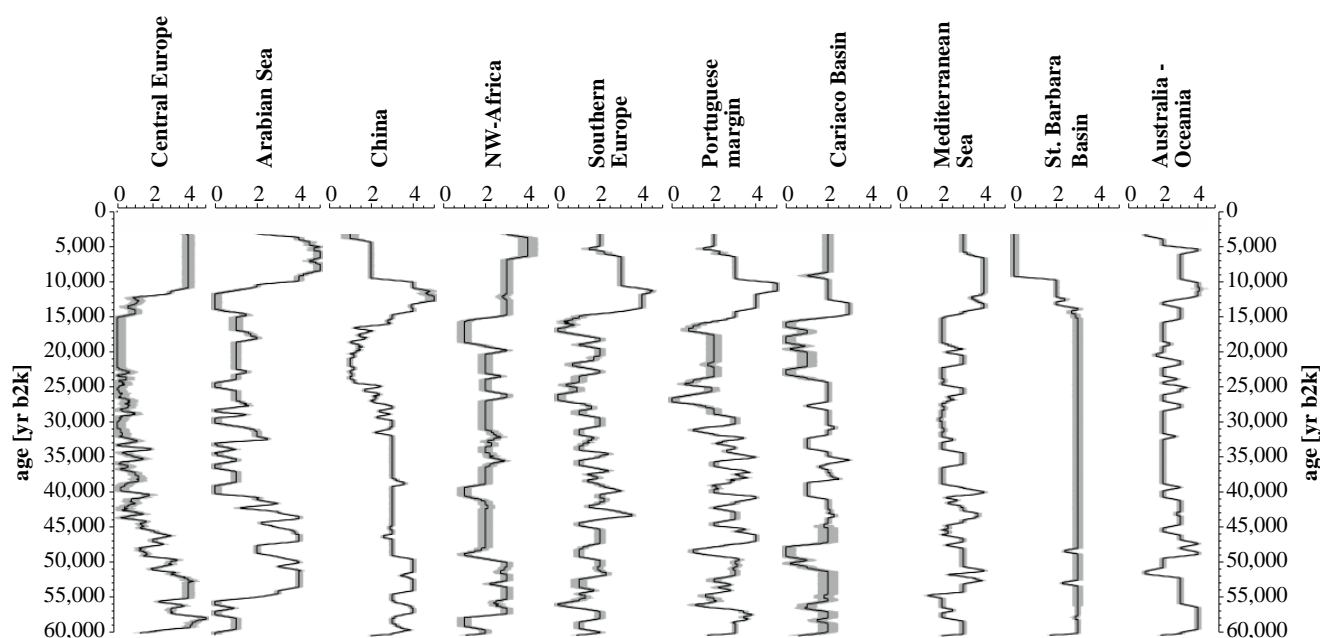
Figure 3: Aridity indices for the 10 key regions over the last 60 000 years. Smaller values indicate more arid, higher values indicate more humid conditions. An early MIS3 wet phase and a Holocene wet phase on various timings for the regions are recognisable.

5   Figure 3 displays all aridity indices from the regional syntheses. Each of them can be found in the related chapters (3.1 and S1-S9) with belonging information. Higher values between 3.5 and 5 show more humid conditions, 3.5 – 1.5 show intermediate precipitation and values below 1.5 accounts for more arid conditions. Humid early MIS 3 is apparent for all regions beside Cariaco Basin and St. Barbara Basin, regarding various timings. Arid LGM conditions are identifiable for Central Europe, Arabian Sea, China, NW-Africa, Southern Europe, Portuguese margin, Cariaco Basin and Mediterranean

10   Sea region. The last deglaciation is visible in all records by drastic changes around 14 700 yr b2k. A humid phase during Holocene is also apparent for all regions, apart from St. Barbara Basin, where the proxies act inversely to the other archives due to regional effects (see S8 'St. Barbara Basin').

Figure 4 is based on the aridity indices shown in Fig. 3 and additional information of the regional syntheses (see Fig. 2 and S1-S9). For example, Chinese Holocene pollen reconstructions (Stebich et al., 2015) give additional information on the

15   Sihailongwan maar lake (see S3 'China'). Also, Reflectance data for Arabian Sea, and Cariaco Basin, XRF data (Cariaco Basin) and the interpretation of the isotope values of the included speleothems are used for this aridity reconstruction. Blue bars show humid, yellow bars intermediate and red bars arid conditions. Transitions or subdivisions between these states are marked by both bars overlapping each other.

Figure 3 shows three large scale structures that link all 10 key areas. The Holocene is in general always relatively humid, but

20   regional variations occur between the early and late Holocene. The LGM is arid in all regions of the globe, but the begin of

the arid phase starts with large offsets between continents and regions. The early MIS3 is quite warm and humid in Europe, south-eastern Asia and Australia, indicating teleconnections between the North Atlantic and the subtropical monsoons.

High humidity is clearly visible for early MIS3 phase for most of the regions apart of the Cariaco basin. The signal is strongest in Central Europe from 60 000 to 48 000 yr b2k, and in the Arabian Sea from 55 000 to 42 000 yr b2k (Fig. 4 and

5   S1). North-west Africa was less humid in the early MIS3, but still shows enhanced precipitation compared to mid and late MIS3. China and Southern Europe were humid. Portuguese margin region underwent larger changes compared to the other regions, as directly influenced by the North Atlantic. The Mediterranean Sea region also was more humid during mid and late MIS3 but not as humid as other regions, St. Barbara Basin shows humidity with same intensity. The Oceania region shows similar patterns for early MIS3 but with a major decrease in precipitation between 55 000 and 50 000 yr b2k. The

10   early MIS3 was generally quite humid in the northern hemisphere. A pronounced aridification occurred with H5 (around 48 000 yr b2k), especially in NW-Africa, Arabian Sea and Europe. The migration of the anatomic modern human can thus be explained by a drag of Europe or an aridity induced push from Africa and Near East.

The time between 45 000 and 15 000 years b2k was globally less humid than the early MIS3 around 50 000 years b2k. Variations occur within the regions during late MIS3, but nevertheless on intermediate or more arid conditions. Heinrich

15   events appear to have a strong impact, especially in the Cariaco Basin where climatic conditions drastically impair during Heinrich events. Towards LGM time, all regions show arid or intermediate conditions, but most arid was again central Europe and the Arabian Sea. The LGM is strongly expressed by decreased precipitation, which is clearly visible within Figure 3 by the red bars around 20 000 years b2k. Oceania conversely shows intermediate values throughout the whole LGM indicating at least some precipitation during the whole period.

20   Following the LGM, a global climate amelioration took place, again with different timings in the onset for each region due to regional or latitudinal effects. The earliest and most drastic climate improvement took place in China, followed shortly by the Mediterranean region, Central Europe, Southern Europe and Portuguese margin. Also, Cariaco Basin, St. Barbara Basin and Oceania underwent climate improvements even bevor the Holocene begun. This climate improvement could be explained by the Bølling / Allerød (14 700 yr b2k). The Altithermal (Early Holocene Climate Optimum / EHTO) took place

25   with begin of the Holocene with a temperature and precipitation maximum around 8 000 years b2k (Shakun and Carlson, 2010). This is apparent for Central Europe, Arabian Sea, north-west Africa, Mediterranean Sea, China as well as Australia - Oceania.
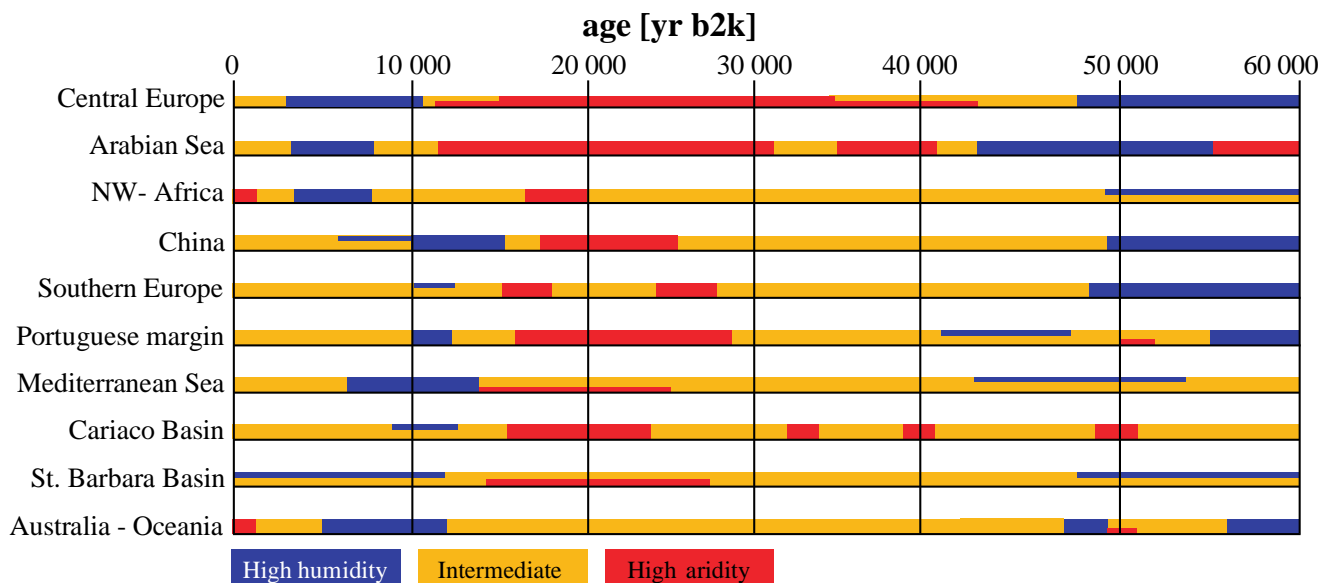
Figure 4: Aridity synthesis for the 10 key regions for the last 60 000 years. Blue bars indicate high humidity, yellow bars intermediate humidity and red bars indicate high humidity. Overlapping half bars indicate transitions between both states. An early MIS3 wet phase and a Holocene wet phase on various timings for the regions are recognisable.

4 Discussion: Global synthesis of speleothems and dust pattern

4.1 Global speleothem growth pattern

Figure 5 summarizes all speleothem growth phases mentioned in the regional syntheses. A consistent pattern shows growth of most speleothems during early MIS3 phase, apart from the Bahamas speleothem standing for the Cariaco Basin where speleothem growth started at about 45 000 years b2k. Except for New Zealand, all regions indicate fast growth rates and corresponding humid conditions at least during interstadials. New Zealand shows low growth rates indicating in general more arid conditions. A major change occurs around HE5, shortly after between 48 000 and 45 000 yr b2k respectively. Speleothem growth stopped in Central Europe caves as well as in Arabian Sea region and drastically slowed down in Southern Europe, China and Mediterranean Sea region during late MIS3. The still fast growth for Cariaco Basin could be explained by a regional effect: enhanced moisture supply due to the position of the speleothem on the Bahamas. Climatic conditions impair with progressing time, growth stopped in Cariaco region as well around 23 000 yr b2k. No growth is observed during LGM times for several regions including Central Europe, Arabian Sea, Southern Europe and Cariaco Basin and very slow growth rates are observed for north-west Africa, China and Mediterranean region pointing out to more arid conditions during late MIS3 and LGM times compared to early MIS3 conditions. This also previously observed effect of large-scale atmospheric teleconnections can also be seen by the onset of Bølling / Allerød (14 700 yr b2k) or after YD (11 703 yr b2k), with the restart of speleothem growth for Central Europe, Arabian Sea, Southern Europe, Cariaco Basin and

accelerating growth rates like for China, Mediterranean region and Santa Barbara Basin region. The available data show climatic amelioration after LGM globally but especially on the northern hemisphere (NH). Oceania and Southern hemisphere (SH) seem to act as a counterpart towards the NH. Fast growth rates in Oceania correspond to no or slow growth rates on the northern hemisphere until the Holocene, where both hemispheres show enhanced moisture supply. This shows reverse

5   behaviour between the climate of the hemispheres: If NH receives more precipitation, SHs precipitation decreases and vice versa.
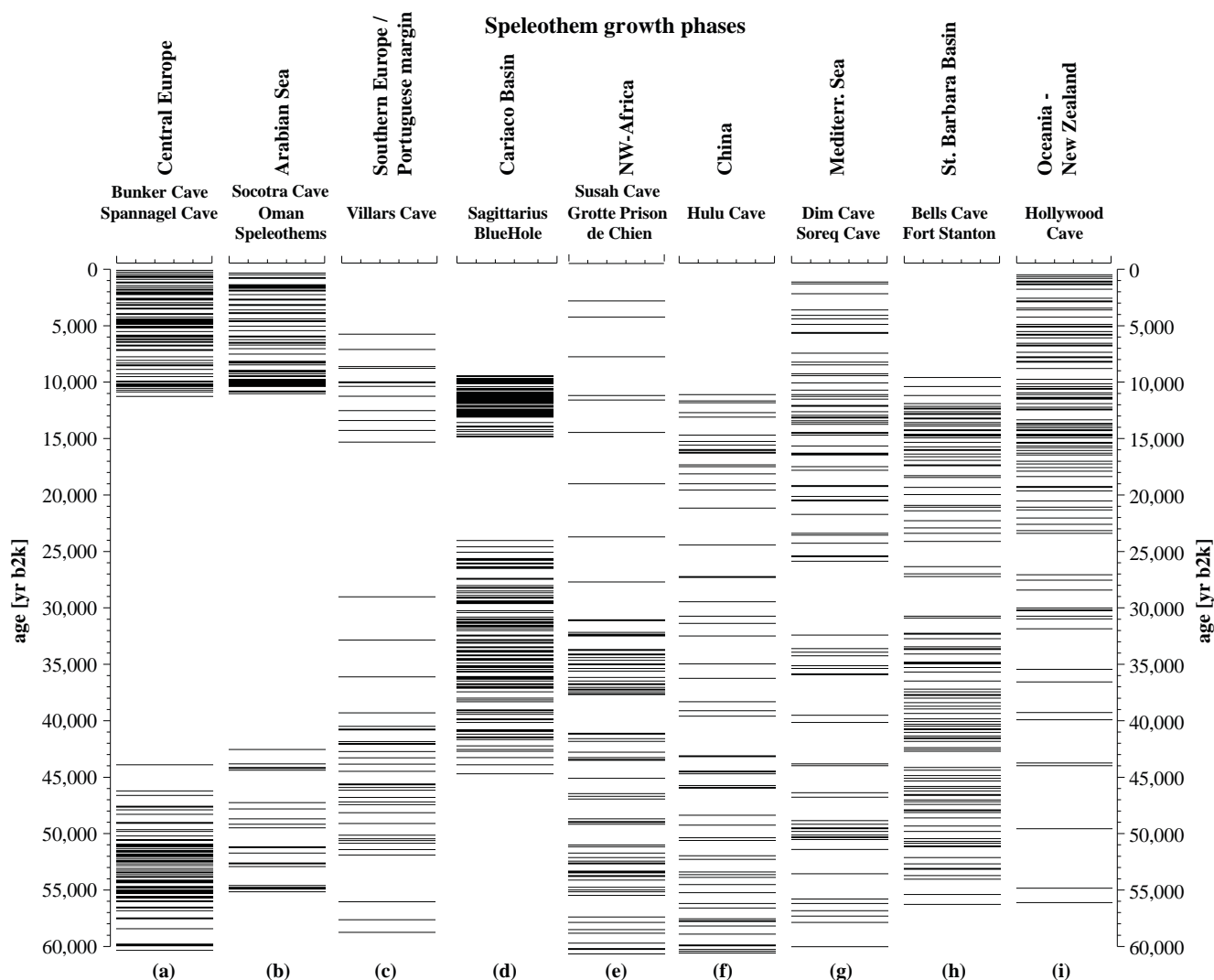
Figure 5: Speleothem growth phases, which require mobile water from frequent precipitation for the 10 key regions. Horizontal bars show age datings. **(a)** Central Europe with Bunker Cave and Spannagel Cave (Fohlmeister et al., 2012, 2013; Holzkämper et al., 2004;
10   Spötl and Mangini, 2002; Weber et al., 2018); **(b)** Socotra Cave and Oman Caves from Arabian Sea region (Burns et al., 2003; Fleitmann et al., 2007); **(c)** Southern Europe and Portuese margin regions represented by Villars Cave speleothems (Genty et al., 2003, 2006; Wainer et al., 2009); **(d)** Sagittarius Blue Hole Bahamas speleothem for Cariaco Basin region (Hoffmann et al., 2010); **(e)** North-West Africa with Grotte Prison de Chien and Susah Cave (Hoffmann et al., 2016; Wassenburg et al., 2012); **(f)** China with Hulu Cave (Liu et al., 2010; Wang et al., 2001); **(g)** Mediterranean Sea region with Dim Cave and Soreq Cave (Bar-Matthews et al., 1997; Ünal-İmer et al.,

2015); **(h)** Bells Cave and Fort Stanton representing St. Barbara Basin (Asmerom et al., 2010; Wagner et al., 2010); **(i)** Hollywood Cave from New Zealand for Oceania region (Hellstrom et al., 1998; Whittaker et al., 2011; Williams, 1996; Williams et al., 2005).

4.2 Global eolian dust pattern
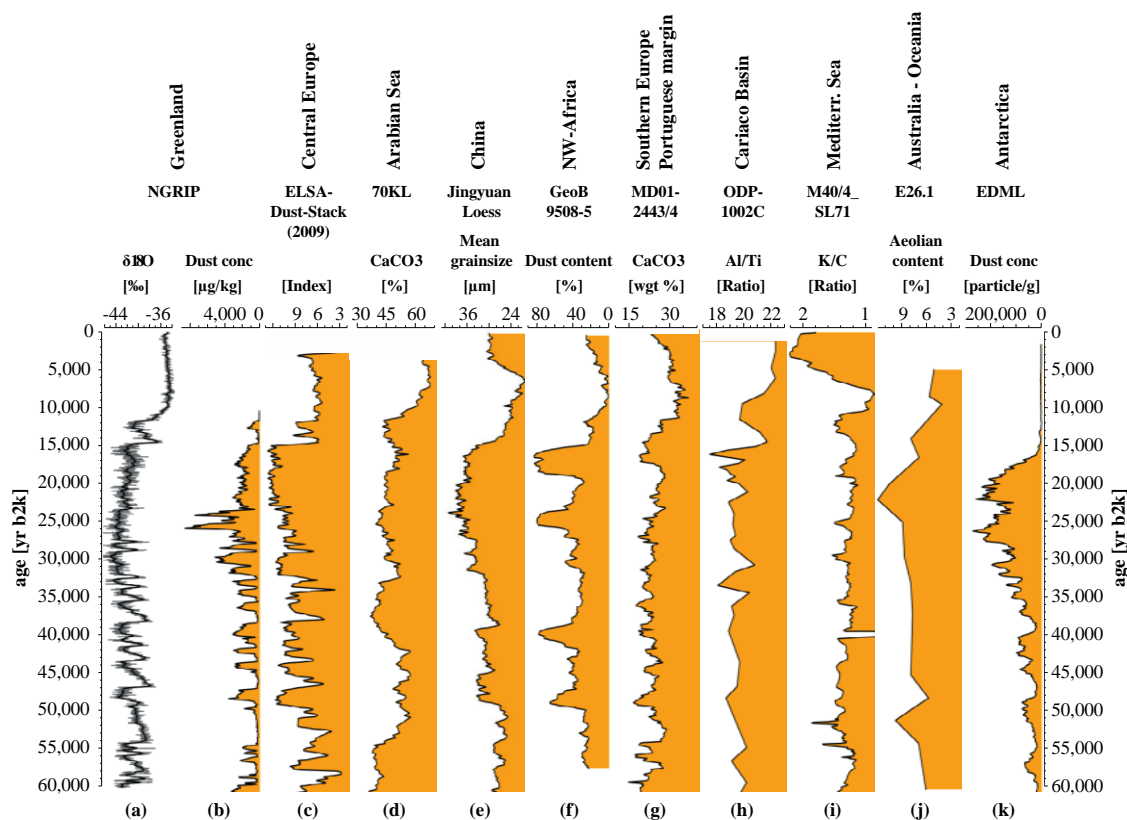
5 **Figure 6: Global eolian dust archives over the last 60 000 years**. More dust (left side of each column) indicates increased aridity, less dust indicates increased humidity. **(a)** NGRIP δ^{18}O (North Greenland Ice Core Project Members et al., 2004) in comparison and **(b)** Dust concentration (Ruth et al., 2007); **(c)** ELSA-Dust-Stack (2009) for Central European dust (Seelos et al., 2009); **(d)** CaCO$_3$ accounting for dust from Arabian Sea marine core 70KL (Leuschner and Sirocko, 2003); **(e)** Mean Grainsize from Jingyuan Chinese Loess plateau (Sun et al., 2010); **(f)** Dust content within marine core GeoB9508-5 off North-West Africa (Collins et al., 2013); **(g)** CaCO$_3$ for Southern Europe
10 and Portuguese margin from marine core MD01-2443/4 (Hodell et al., 2013) **(h)** Cariaco Basin Al/Ti ratio dust record from marine core ODP-165-1002C (Yarincik et al., 2000); **(i)** K/C ratio from marine core M40/4_SL71 for Mediterranean Sea **(Ehrmann et al., 2017)**; **(j)** Aeolian content from marine core E26.1 from Tasmanian Sea for Oceania (Hesse, 1994); **(k)** Antarctica ice core EDML Dust concentration (Wegner et al., 2015) in comparison.

Similar patterns are visible in the dust archives used for this synthesis. For early MIS3, low dust values are discernible for

15 Central Europe, China, north-west Africa and intermediate dust values for all other regions beside the Arabian Sea. In general, MIS3 climate shows flickering visible within the dust records.

Apart from every region's own pattern, some background structures are apparent. Heinrich events are most pronounced for NW-Africa, Cariaco Basin, Southern Europe and Portuguese margin regions, as these regions directly belong to the North Atlantic. Mediterranean Sea, Central Europe and China also show Heinrich events within the dust records. Cariaco Basin,

China, Arabian Sea, NW-Africa and Central Europe show a distinct dust maximum during LGM. Beside during Holocene, the lowest dust values are apparent in the early MIS3 for Central Europe, Arabian Sea, China, NW-Africa and Mediterranean Sea – but on various timings. NGRIP dust concentration and ELSA-Dust-Stack (Seelos et al., 2009) are in good accordance for early and mid MIS3. Turning points show stepped appearance in both archives at several times (~49 000, ~36 500, ~23 000, ~14 700 yr b2k) which are also visible and described as Landscape Evolution Zones (LEZ) in Sirocko et al. (2016). The good consistency of both regions indicates a close connection to the North-Atlantic climate variations. Arabian Sea sediments also are closely coupled to North Atlantic variability as known since Schultz et al. (1998) and visible within Fig. 6.

Sun et al. (2010) also shows a correlation of Chinese loess to North Atlantic climate variations. High dust contents during mid MIS3 and LGM are visible in most archives, often related to dustier Heinrich events or stadials in general. Increasing dust values around 30 000 yr b2k towards the LGM show nearly global distribution, but regional differences are observable: ELSA-Dust-Stack and NGRIP differ in the timing of maximum dust values. This could be explained by a similar process like blocking of westerly winds by ice shield growth which is described in Schenk (Schenk et al., 2018) and Schiemann (Schiemann et al., 2017).

From 30 000 to 17 000 yr b2k, the conditions were mainly arid, discernible by the dust maxima in Greenland, Central Europe, China, Portuguese margin, Australia - Oceania and Antarctica for LGM. With the YD and the onset towards the Holocene, global climate ameliorates and dust values decrease globally until the end of the Altithermal. Afterwards, dust increases in Arabian Sea, China, NW-Africa, Portuguese margin and Mediterranean Sea indicating increased aridification of the large desert areas in Africa, Arabian Peninsula and China (Gobi). Large changes occurred simultaneously on the globe during the last 60 000 years of climate history indicating atmospheric teleconnections (Bjerknes, 1969; Markle et al., 2017; Sirocko, 2003; Sirocko et al., 1996; Zhou et al., 1999).

4.2 Comparison of aridity index and previous aridity reconstruction

Aridity reconstructions of Herzschuh (Herzschuh, 2006) for the last 50 000 years for Central Asia are in excellent agreement to the aridity reconstructions of this synthesis of the China region (S3). Herzschuh solely used pollen data for the reconstruction, while our aridity index is based on three distinct proxies to refine the picture. The aridity index in addition consists of longer records and reaches until the beginning of MIS3 (60 000 yr b2k). It shows a humid early MIS3 and a decrease in humidity around 50 000 yr b2k to intermediate conditions. Moderate dry conditions are reconstructed for 50 000 to 45 000 yr b2k from Herzschuh, similar to the aridity index, followed by an increase in humidity until 40 000 yr b2k. Minor differences between 45 000 and 30 000 yr b2k are apparent, but the general trend shows broad consensus between both reconstructions for this time. Mid to late MIS3 are relatively humid in both reconstructions. Aridity increases drastically towards the LGM in both reconstructions with a strong LGM aridity maximum from 21 000 to 18 000 yr b2k. Stepwise climate amelioration after the LGM is clearly expressed in both reconstructions, a first increase in humidity occurs until 13 000 yr b2k with following optimal climate conditions during early Holocene (11 000 - 7 000 yr b2k). The aridity index

lacks in Holocene data (see S3) but the accordance of Herzschuh compared to published Holocene pollen data of Stebich (Stebich et al., 2015) is evident and shows an early Holocene climate optimum until 4 000 yr b2k in both reconstructions. A wet early Holocene can be observed at Central Chinese speleothem growth rates from 'Sanbao Cave', which are fastest from 9 500 to 6 500 yr b2k (Dong et al., 2010).

4.3 Comparison of proxy synthesis with model results

The above records describe the structure of past aridity globally, but do not present causal mechanism, which

Global Climate Models (GCM) can be used to simulate past, present and future climate changes. In order to our reconstructed precipitation with the large-scale pattern of model simulation, we employ the coupled climate model COSMOS which was developed at the Max-Planck Institute for Meteorology in Hamburg (Jungclaus et al., 2010). The model has been successfully applied to test a variety of paleoclimate hypotheses, ranging from the Miocene climate (Knorr et al., 2011; Knorr and Lohmann, 2014; Stein et al., 2016), the Pliocene (Stepanek and Lohmann, 2012) as well as glacial (Abelmann et al., 2015; Gong et al., 2013; Zhang et al., 2013) and interglacial climates (Lohmann et al., 2013; Pfeiffer and Lohmann, 2016; Wei and Lohmann, 2012). Here, we use a combination of various model simulations with COSMOS for pre-industrial (Wei and Lohmann, 2012), LGM (Zhang et al., 2013) and late MIS3 (32 000 yr b2k) simulations (Gong et al., 2013). The simulations have been run for over 2000-year time period to reach their respective quasi-equilibrium states. Orbital forcing is inferred from Berger (Berger, 1978), the greenhouse gas concentrations from ice cores and the ice sheet configurations are described in detail in Gong et al. (2013). For the late MIS3, the model mimics a GS due to freshwater hosing and GI with an overshoot in temperature (Gong et al., 2013). Fig. 7 displays precipitation changes and anomalies from Late MIS3 time slice with respect to pre-industrial (PI) and LGM conditions. Panel A and C show stadial conditions and panels B and D show interstadial conditions. Panels A and B show the 32 000 yr b2k time slice with respect to pre-industrial times while panels C and D are with respect to LGM conditions.

Model runs for late MIS3 interstadial times show enhanced precipitation for Europe, North Atlantic, Arabian Sea and large parts of the equatorial Pacific, while remaining parts of equator in Asia, Central Atlantic and northern parts of South America show decreased precipitation. Stadial MIS3 state in general shows the same spacious trends but with general higher aridity. Model and aridity reconstructions match in nearly equal conditions for PI and MIS3. Barron and Pollard (Barron and Pollard, 2002) simulated a 42 000 yr b2k time slice for European precipitation. The results are comparable to our aridity index, but Central Europe, Southern Europe and Portuguese margin were more humid in our reconstruction than in the simulation. In contrast, these results show that the 42 000 yr b2k time slice was more humid than 32 000 yr b2k time slice for Europe. Our reconstruction estimates precipitation even higher during early and mid than during late MIS3 and to be as high as during early Holocene optimum. This could be said for all regions beside the Cariaco Basin, regarding the different timings of the wet periods. In current models, late MIS3 and especially comparisons between the early and late MIS3 were not investigated so far.
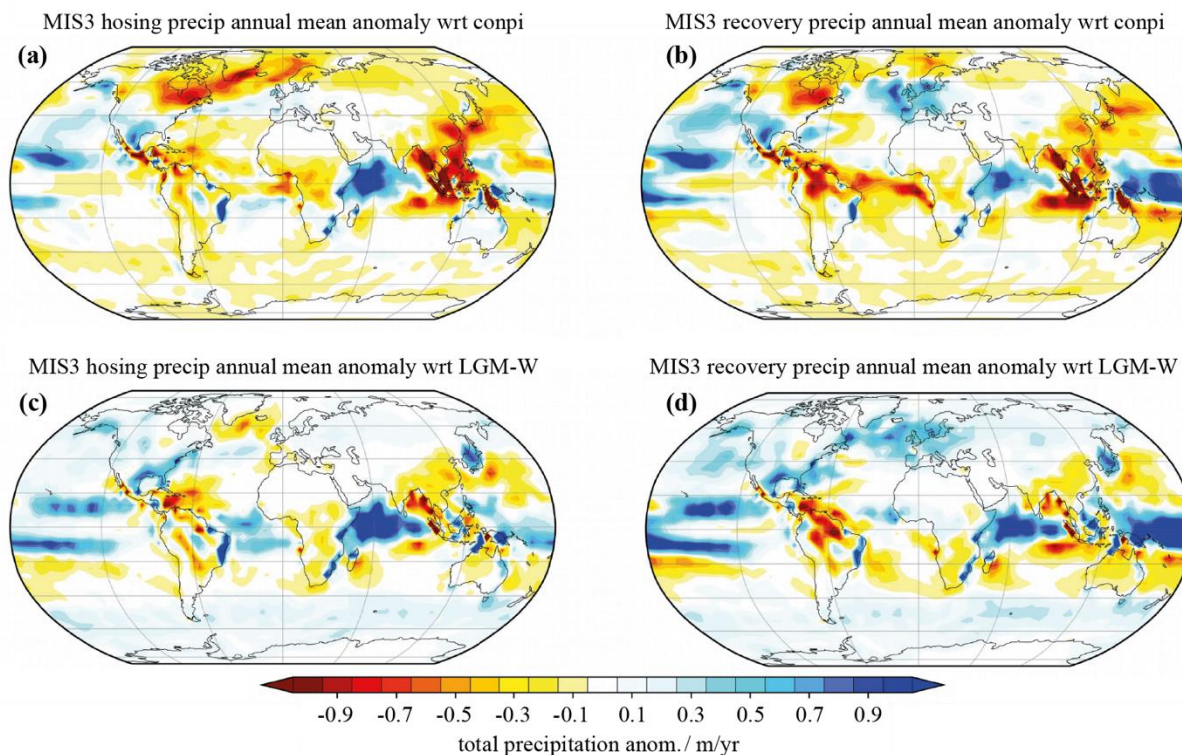
Figure 7: Simulated total precipitation anomalies for the late MIS3 climate relative to pre-industrial times (a, b) or LGM (c, d).
Panel **(a, c)** show stadial conditions (hosing) and panels **(b, d)** show interstadial conditions (recovery). Simulation is compiled of various model simulations with COSMOS for pre-industrial (Wei and Lohmann, 2012), LGM (Zhang et al., 2013) and Late MIS3 (32 000 yr b2k) simulations (Gong et al., 2013).

	MIS 3 wrt. PI		MIS 3 wrt. LGM	
	32 000 [a]		32 000 [a]	
	GS	GI	GS	GI
Central Europe	o	+	o	+
Southern Europe	+	+	o	+
Portuguese margin	o	+	o	o
Mediterranean Sea	o	o	o	o
NW Africa	o	o	o	o
China	-	-	-	o
Arabian Sea	+	+	+	o
Cariaco basin	-	-	-	-
St. Barbara basin	o	o	o	o
Australia - Oceania	o	o	o	o

Table 3. Comparison of model simulation with reconstructed aridity index. Relatively larger aridity with respect to PI or LGM for each region is shown with a minus (-), approximately the same conditions with an open circle (o) and more humid conditions with a small plus (+). Bad agreement of simulation and aridity index is shown with red colour, medium by yellow colour, light and intense green account for good or even better accordance respectively.

Table 3 summarizes results from the model simulations from Fig. 7, converted into symbols. This model setup is divided in GI and GS state and is compared with the results for the aridity reconstructions from Fig. 4 for each of the ten key regions. Relatively larger aridity with respect to PI or LGM for each region is shown with a minus (-), approximately the same conditions with a circle (o) and more humid conditions with a small plus (+). The agreement of each simulation and the aridity reconstructions of this work is shown in addition. Bad congruence is displayed in red colour, medium with yellow and light and intense green for good and even better accordance respectively. The overall consistence of model and reconstruction is good. Most of the precipitation changes of the aridity index are observable in the simulation as well.

The aridity reconstructions show that Central Europe was humid during early MIS3, followed by an intermediate to highly arid period until the end of LGM.

5 Conclusions

The aridity synthesis for the ten key regions of the world's climate allows six main conclusions to be drawn:

(1) All regions gone through a phase of large humidity during early MIS3, as well as phase of large humidity during the early Holocene. The timing of this humid MIS3 phase varied considerable from region to region.

(2) Atmospheric teleconnections occurred from North Atlantic (Greenland) over Central Europe, Arabian Sea until China. The changes in these regions took place within similar timings and with similar strength. The other regions also went through these changes but with differences in timing. We attribute this to indeed regional effects rather than simply dating uncertainties.

(3) Eolian dust, tree pollen and speleothem growth phases show congruent climatic pattern for the individual regions and can be compared easily regarding precipitation analyses.

(4) The aridity index and the precipitation simulations are generally consistent.

(5) The quality of the aridity index is limited mostly by the original stratigraphy and sample resolution. It is accordingly a useful tool to observe large scale precipitation changes.

(6) The aridity suggests a general antiphase behaviour between LGM and early MIS3 for northern hemisphere and Australia - Oceania.

Author contributions

FF generated the aridity index, processed the data and prepared the manuscript. GL and XG developed and performed the climate simulation. BD greatly improved the error simulations and aridity reconstruction measurements. FS and XG improved the manuscript with their contributions.

Acknowledgments

This work was supported by German Federal Ministry of Education and Research (BMBF) as Research for Sustainability initiative (FONA); www.fona.de through PalMod project (FKZ: 01LP1510B). The authors would like to thank Manfred Mudelsee for input on the error estimations, Philip Süßer and Jennifer Klose for data mining, Hannes Knapp, Michael Weber Johannes Albert, Sarah Britzius, Klaus Schwibus and Frank Dreher for their fruitful contributions as well as all colleagues, who contributed data.

References

Abelmann, A., Gersonde, R., Knorr, G., Zhang, X., Chapligin, B., Maier, E., Esper, O., Friedrichsen, H., Lohmann, G., Meyer, H. and Tiedemann, R.: The seasonal sea-ice zone in the glacial Southern Ocean as a carbon sink, Nature Communications, 6, 8136, doi:10.1038/ncomms9136, 2015.

Andersen, K. K., Svensson, A., Johnsen, S. J., Rasmussen, S. O., Bigler, M., Röthlisberger, R., Ruth, U., Siggaard-Andersen, M.-L., Peder Steffensen, J. and Dahl-Jensen, D.: The Greenland Ice Core Chronology 2005, 15–42ka. Part 1: constructing the time scale, Quaternary Science Reviews, 25(23–24), 3246–3257, doi:10.1016/j.quascirev.2006.08.002, 2006.

Asmerom, Y., Polyak, V. J. and Burns, S. J.: Variable winter moisture in the southwestern United States linked to rapid glacial climate shifts, Nature Geoscience, 3(2), 114–117, doi:10.1038/ngeo754, 2010.

Bar-Matthews, M., Ayalon, A. and Kaufman, A.: Late Quaternary Paleoclimate in the Eastern Mediterranean Region from Stable Isotope Analysis of Speleothems at Soreq Cave, Israel, Quaternary Research, 47(2), 155–168, doi:10.1006/qres.1997.1883, 1997.

Barron, E. and Pollard, D.: High-Resolution Climate Simulations of Oxygen Isotope Stage 3 in Europe 1, Quaternary Research, 58(3), 296–309, doi:10.1006/qres.2002.2374, 2002.

Berger, A. L.: Long term variations of caloric solar radiation resulting from the earth's orbital elements, Quaternary Research, 9, 139–167, 1978.

Bintanja, R. and van de Wal, R. S. W.: North American ice-sheet dynamics and the onset of 100,000-year glacial cycles, Nature, 454(7206), 869–872, doi:10.1038/nature07158, 2008.

Bjerknes, J.: Atmospheric teleconnections from the equatorial pacific, Mon. Wea. Rev., 97(3), 163–172, doi:10.1175/1520-0493(1969)097<0163:ATFTEP>2.3.CO;2, 1969.

Bond, G., Showers, W., Cheseby, M., Lotti, R., Almasi, P., deMenocal, P., Priore, P., Cullen, H., Hajdas, I. and Bonani, G.: A pervasive millenial-scale Cycle in the North Atlantic Holocene and Glacial Climates, Nature, 278, 1257–1266, 1998.

Büchel, G.: Vulkanologische Karte der West- und Hocheifel, 1994.

Burns, S. J., Fleitmann, D., Matter, A., Kramers, J. and Al-Subbary A. A: Indian Ocean Climate and a Absolute Chronology over Dansgaard/Oescher Events 9 to 13, Science, 301, 1365–1367, 2003.

Collins, J. A., Govin, A., Mulitza, S., Heslop, D., Zabel, M., Hartmann, J., Röhl, U. and Wefer, G.: Abrupt shifts of the Sahara-Sahel boundary during Heinrich stadials, Climate of the Past, 9(3), 1181–1191, doi:10.5194/cp-9-1181-2013, 2013.

Deutscher Wetterdienst: Wetter und Klima - Deutscher Wetterdienst - Klimadaten weltweit, [online] Available from: https://www.dwd.de/DE/leistungen/klimadatenwelt/klimadatenwelt_node.html (Accessed 17 July 2018), 2018.

Dietrich, S. and Seelos, K.: The reconstruction of easterly wind directions for the Eifel region (Central Europe) during the period 40.3 -12.9 ka BP, Climate of the Past, 6(2), 145–154, doi:10.5194/cp-6-145-2010, 2010.

Dietrich, S. and Sirocko, F.: The potential of dust detection by means of µXRF scanning in Eifel maar lake sediments, Quaternary Science Journal, 60(1), 90–104, doi:10.3285/eg.60.1.06, 2011.

Dong, J., Wang, Y., Cheng, H., Hardt, B., Edwards, R. L., Kong, X., Wu, J., Chen, S., Liu, D., Jiang, X. and Zhao, K.: A high-resolution stalagmite record of the Holocene East Asian monsoon from Mt Shennongjia, central China, The Holocene, 20(2), 257–264, doi:10.1177/0959683609350393, 2010.

Ehrmann, W., Schmiedl, G., Beuscher, S. and Krüger, S.: Intensity of African Humid Periods Estimated from Saharan Dust Fluxes, edited by S.-P. Xie, PLOS ONE, 12(1), e0170989, doi:10.1371/journal.pone.0170989, 2017.

EPICA community members: Eight glacial cycles from an Antarctic ice core, Nature, 429(6992), 623–628, doi:10.1038/nature02599, 2004.

Fleitmann, D., Burns, S. J., Mangini, A., Mudelsee, M., Kramers, J., Villa, I., Neff, U., Al-Subbary, A. A., Buettner, A., Hippler, D. and Matter, A.: Holocene ITCZ and Indian monsoon dynamics recorded in stalagmites from Oman and Yemen (Socotra), Quaternary Science Reviews, 26(1–2), 170–188, doi:10.1016/j.quascirev.2006.04.012, 2007.

Fohlmeister, J., Schröder-Ritzrau, A., Scholz, D., Spötl, C., Riechelmann, D. F. C., Mudelsee, M., Wackerbarth, A., Gerdes, A., Riechelmann, S., Immenhauser, A., Richter, D. K. and Mangini, A.: Bunker Cave stalagmites: an archive for central European Holocene climate variability, Climate of the Past, 8(5), 1751–1764, doi:10.5194/cp-8-1751-2012, 2012.

Fohlmeister, J., Vollweiler, N., Spötl, C. and Mangini, A.: COMNISPA II: Update of a mid-European isotope climate record, 11 ka to present, The Holocene, 23(5), 749–754, doi:10.1177/0959683612465446, 2013.

Genty, D., Blamart, D., Ouahdi, R., Gilmour, M., Baker, A., Jouzel, J. and Van-Exter, S.: Precise dating of Dansgaard–Oeschger climate oscillations in western Europe from stalagmite data, Nature, 421(6925), 833–837, doi:10.1038/nature01391, 2003.

Genty, D., Blamart, D., Ghaleb, B., Plagnes, V., Causse, Ch., Bakalowicz, M., Zouari, K., Chkir, N., Hellstrom, J. and Wainer, K.: Timing and dynamics of the last deglaciation from European and North African δ13C stalagmite profiles—comparison with Chinese and South Hemisphere stalagmites, Quaternary Science Reviews, 25(17–18), 2118–2142, doi:10.1016/j.quascirev.2006.01.030, 2006.

Gong, X., Knorr, G., Lohmann, G. and Zhang, X.: Dependence of abrupt Atlantic meridional ocean circulation changes on climate background states, Geophysical Research Letters, 40(14), 3698–3704, doi:10.1002/grl.50701, 2013.

Grootes, P. M., Stulver, M., White, J. W. C., Johnsen, S. and Jouzel, J.: Comparison of oxygen isotope reccords from the GISP2 and GRIP Greenland ice cores, Nature, 366, 552–554, 1993.

Heinrich, H.: Origin and Consequences of Cyclic Ice Rafting in the Northeast Atlantic Ocean During the Past 130,000 Years, Quaternary Research, 29(2), 142–152, doi:10.1016/0033-5894(88)90057-9, 1988.

Hellstrom, J., McCulloch, M. and Stone, J.: A Detailed 31,000-Year Record of Climate and Vegetation Change, from the Isotope Geochemistry of Two New Zealand Speleothems, Quaternary Research, 50(2), 167–178, doi:10.1006/qres.1998.1991, 1998.

Herzschuh, U.: Palaeo-moisture evolution in monsoonal Central Asia during the last 50,000 years, Quaternary Science Reviews, 25(1), 163–178, doi:10.1016/j.quascirev.2005.02.006, 2006.

Hesse, P. P.: The record of continental dust from Australia in Tasman Sea Sediments, Quaternary Science Reviews, 13(3), 257–272, doi:10.1016/0277-3791(94)90029-9, 1994.

Hodell, D., Crowhurst, S., Skinner, L., Tzedakis, P. C., Margari, V., Channell, J. E. T., Kamenov, G., Maclachlan, S. and Rothwell, G.: Response of Iberian Margin sediments to orbital and suborbital forcing over the past 420 ka, Paleoceanography, 28(1), 185–199, doi:10.1002/palo.20017, 2013.

Hoffmann, D. L., Beck, J. W., Richards, D. A., Smart, P. L., Singarayer, J. S., Ketchmark, T. and Hawkesworth, C. J.: Towards radiocarbon calibration beyond 28ka using speleothems from the Bahamas, Earth and Planetary Science Letters, 289(1–2), 1–10, doi:10.1016/j.epsl.2009.10.004, 2010.

Hoffmann, D. L., Rogerson, M., Spötl, C., Luetscher, M., Vance, D., Osborne, A. H., Fello, N. M. and Moseley, G. E.: Timing and causes of North African wet phases during the last glacial period and implications for modern human migration, Scientific Reports, 6, 36367, doi:10.1038/srep36367, 2016.

Holzkämper, S., Mangini, A., Spötl, C. and Mudelsee, M.: Timing and progression of the Last Interglacial derived from a high alpine stalagmite: TIMING OF THE LAST INTERGLACIAL, Geophysical Research Letters, 31(7), n/a-n/a, doi:10.1029/2003GL019112, 2004.

Jungclaus, J. H., Lorenz, S. J., Timmreck, C., Reick, C. H., Brovkin, V., Six, K., Segschneider, J., Giorgetta, M. A., Crowley, T. J., Pongratz, J., Krivova, N. A., Vieira, L. E., Solanki, S. K., Klocke, D., Botzet, M., Esch, M., Gayler, V., Haak, H., Raddatz, T., Roeckner, E., Schnur, R., Widmann, H., Claussen, M., Stevens, B. and Marotzke, J.: Climate and carbon-cycle variability over the last millennium, Climate of the Past, 6, 723–737, doi:10.5194/cp-6-723-2010, 2010.

Kindler, P., Guillevic, M., Baumgartner, M., Schwander, J., Landais, A., Leuenberger, M., Spahni, R., Capron, E. and Chappellaz, J.: Temperature reconstruction from 10 to 120 kyr b2k from the NGRIP ice core, Climate of the Past, 10(2), 887–902, doi:10.5194/cp-10-887-2014, 2014.

Knorr, G. and Lohmann, G.: Climate warming during Antarctic ice sheet expansion at the Middle Miocene transition, Nature Geoscience, 7(5), 376–381, doi:10.1038/ngeo2119, 2014.

Knorr, G., Butzin, M., Micheels, A. and Lohmann, G.: A warm Miocene climate at low atmospheric CO2 levels, Geophysical Research Letters, 38(20), doi:10.1029/2011GL048873, 2011.

Koehler, E., Brown, E. and Haneuse, S. J.-P. A.: On the Assessment of Monte Carlo Error in Simulation-Based Statistical Analyses, Am Stat, 63(2), 155–162, doi:10.1198/tast.2009.0030, 2009.

Leuschner, D. C. and Sirocko, F.: Orbital insolation forcing of the Indian Monsoon - a motor for global climate changes?, Palaeogeography Palaeoclimatology Palaeoecology, 197(1–2), 83–95, 2003.

Litt, T. and Stebich, M.: Bio- and chronostratigraphy of the lateglacial in the Eifel region, Germany, Quaternary International, 61(1), 5–16, doi:10.1016/S1040-6182(99)00013-0, 1999.

Liu, D., Wang, Y., Cheng, H., Lawrence Edwards, R., Kong, X., Wang, X., Hardt, B., Wu, J., Chen, S., Jiang, X., He, Y., Dong, J. and Zhao, K.: Sub-millennial variability of Asian monsoon intensity during the early MIS 3 and its analogue to the ice age terminations, Quaternary Science Reviews, 29(9), 1107–1115, doi:10.1016/j.quascirev.2010.01.008, 2010.

Lohmann, G., Pfeiffer, M., Laepple, T., Leduc, G. and Kim, J.-H.: A model-data comparison of the Holocene global sea surface temperature evolution, Climate of the Past, 1807–1839, doi:Lohmann, G. ORCID: https://orcid.org/0000-0003-2089-733X <https://orcid.org/0000-0003-2089-733X>, Pfeiffer, M. , Laepple, T. ORCID: https://orcid.org/0000-0001-8108-7520 <https://orcid.org/0000-0001-8108-7520>, Leduc, G. and Kim, J. H. (2013) A model-data comparison of the Holocene global sea surface temperature evolution , Climate of the Past, (9), pp. 1807-1839 . doi:https://doi.org/10.5194/cp-9-1807-2013 <https://doi.org/10.5194/cp-9-1807-2013> , hdl:10013/epic.41917, 2013.

Markle, B. R., Steig, E. J., Buizert, C., Schoenemann, S. W., Bitz, C. M., Fudge, T. J., Pedro, J. B., Ding, Q., Jones, T. R., White, J. W. C. and Sowers, T.: Global atmospheric teleconnections during Dansgaard–Oeschger events, Nature Geoscience, 10(1), 36–40, doi:10.1038/ngeo2848, 2017.

McManus, J. F., Bond, G. C., Broecker, W. S., Johnsen, S., Labeyrie, L. and Higgins, S.: High-resolution climate records from the North Atlantic during the last interglacial, Nature, 371(6495), 326, doi:10.1038/371326a0, 1994.

Naafs, B. D. A., Hefter, J., Grützner, J. and Stein, R.: Warming of surface waters in the mid-latitude North Atlantic during Heinrich events: HIGH SSTs DURING HEINRICH EVENTS, Paleoceanography, 28(1), 153–163, doi:10.1029/2012PA002354, 2013.

Negendank, J. F. W.: Pleistozäne und holozäne Maarsedimente der Eifel, Zeitschrift der Deutschen Geologischen Gesellschaft, 13–24, 1989.

North Greenland Ice Core Project Members, Andersen, K. K., Azuma, N., Barnola, J.-M., Bigler, M., Biscaye, P., Caillon, N., Chappellaz, J., Clausen, H. B., Dahl-Jensen, D., Fischer, H., Flückiger, J., Fritzsche, D., Fujii, Y., Goto-Azuma, K., Grønvold, K., Gundestrup, N. S., Hansson, M., Huber, C., Hvidberg, C. S., Johnsen, S. J., Jonsell, U., Jouzel, J., Kipfstuhl, S., Landais, A., Leuenberger, M., Lorrain, R., Masson-Delmotte, V., Miller, H., Motoyama, H., Narita, H., Popp, T., Rasmussen, S. O., Raynaud, D., Rothlisberger, R., Ruth, U., Samyn, D., Schwander, J., Shoji, H., Siggard-Andersen, M.-L., Steffensen, J. P., Stocker, T., Sveinbjörnsdóttir, A. E., Svensson, A., Takata, M., Tison, J.-L., Thorsteinsson, T., Watanabe, O., Wilhelms, F. and White, J. W. C.: High-resolution record of Northern Hemisphere climate extending into the last interglacial period, Nature, 431(7005), 147–151, doi:10.1038/nature02805, 2004.

Pfeiffer, M. and Lohmann, G.: Greenland Ice Sheet influence on Last Interglacial climate: global sensitivity studies performed with an atmosphere–ocean general circulation model, Climate of the Past, 1313–1338, 2016.

Pye, K.: Aeolian dust and dust deposits., Academic Press, University of Cambridge., 1987.

Rasmussen, S. O., Andersen, K. K., Svensson, A. M., Steffensen, J. P., Vinther, B. M., Clausen, H. B., Siggaard-Andersen, M.-L., Johnsen, S. J., Larsen, L. B., Dahl-Jensen, D., Bigler, M., Röthlisberger, R., Fischer, H., Goto-Azuma, K., Hansson, M. E. and Ruth, U.: A new Greenland ice core chronology for the last glacial termination, Journal of Geophysical Research, 111(D6), doi:10.1029/2005JD006079, 2006.

Rasmussen, S. O., Bigler, M., Blockley, S. P., Blunier, T., Buchardt, S. L., Clausen, H. B., Cvijanovic, I., Dahl-Jensen, D., Johnsen, S. J., Fischer, H., Gkinis, V., Guillevic, M., Hoek, W. Z., Lowe, J. J., Pedro, J. B., Popp, T., Seierstad, I. K., Steffensen, J. P., Svensson, A. M., Vallelonga, P., Vinther, B. M., Walker, M. J. C., Wheatley, J. J. and Winstrup, M.: A

stratigraphic framework for abrupt climatic changes during the Last Glacial period based on three synchronized Greenland ice-core records: refining and extending the INTIMATE event stratigraphy, Quaternary Science Reviews, 106, 14–28, doi:10.1016/j.quascirev.2014.09.007, 2014.

Ruth, U., Wagenbach, D., Steffensen, J. P. and Bigler, M.: Continuous record of microparticle concentration and size distribution in the central Greenland NGRIP ice core during the last glacial period: CONTINUOUS RECORD OF MICROPARTICLE CONCENTRATION, Journal of Geophysical Research: Atmospheres, 108(D3), n/a-n/a, doi:10.1029/2002JD002376, 2003.

Ruth, U., Bigler, M., Röthlisberger, R., Siggaard-Andersen, M.-L., Kipfstuhl, S., Goto-Azuma, K., Hansson, M. E., Johnsen, S. J., Lu, H. and Steffensen, J. P.: Ice core evidence for a very tight link between North Atlantic and east Asian glacial climate, Geophysical Research Letters, 34(3), doi:10.1029/2006GL027876, 2007.

Schaber, K. and Sirocko, F.: Lithologie und Stratigraphie der spätpleistozänen Trockenmaare der Eifel, Mainzer geowissenschaftliche Mitteilungen, 33, 295–340, 2005.

Schenk, F., Väliranta, M., Muschitiello, F., Tarasov, L., Heikkilä, M., Björck, S., Brandefelt, J., Johansson, A. V., Näslund, J.-O. and Wohlfarth, B.: Warm summers during the Younger Dryas cold reversal, Nature Communications, 9(1), doi:10.1038/s41467-018-04071-5, 2018.

Schiemann, R., Demory, M.-E., Shaffrey, L. C., Strachan, J., Vidale, P. L., Mizielinski, M. S., Roberts, M. J., Matsueda, M., Wehner, M. F. and Jung, T.: The resolution sensitivity of Northern Hemisphere blocking in four 25-km atmospheric global circulation models, Journal of Climate, 30, 337–358, 2017.

Schulz, H., von Rad, U., Erlenkeuser, H. and von Rad, U.: Correlation between Arabian Sea and Greenland climate oscillations of the past 110,000 years, Nature, 393(6680), 54–57, doi:10.1038/31750, 1998.

Seelos, K., Sirocko, F. and Dietrich, S.: A continuous high-resolution dust record for the reconstruction of wind systems in central Europe (Eifel, Western Germany) over the past 133 ka, Geophysical Research Letters, 36(20), doi:10.1029/2009GL039716, 2009.

Shakun, J. D. and Carlson, A. E.: A global perspective on Last Glacial Maximum to Holocene climate change, Quaternary Science Reviews, 29(15), 1801–1816, doi:10.1016/j.quascirev.2010.03.016, 2010.

Sirocko, F.: What Drove Past Teleconnections?, Science, 301(5638), 1336–1337, doi:10.1126/science.1088626, 2003.

Sirocko, F.: The ELSA - Stacks (Eifel-Laminated-Sediment-Archive): An introduction, Global and Planetary Change, 142, 96–99, doi:10.1016/j.gloplacha.2016.03.011, 2016.

Sirocko, F., Garbe-Schönberg, D., McIntyre, A. and Molfino, B.: Teleconnections Between the Subtropical Monsoons and High-Latitude Climates During the Last Deglaciation, Science, 272(5261), 526–529, doi:10.1126/science.272.5261.526, 1996.

Sirocko, F., Knapp, H., Dreher, F., Förster, M. W., Albert, J., Brunck, H., Veres, D., Dietrich, S., Zech, M., Hambach, U., Röhner, M., Rudert, S., Schwibus, K., Adams, C. and Sigl, P.: The ELSA-Vegetation-Stack: Reconstruction of Landscape Evolution Zones (LEZ) from laminated Eifel maar sediments of the last 60,000years, Global and Planetary Change, 142, 108–135, doi:10.1016/j.gloplacha.2016.03.005, 2016.

Spötl, C. and Mangini, A.: Stalagmite from the Austrian Alps reveals Dansgaard–Oeschger events during isotope stage 3: Implications for the absolute chronology of Greenland ice cores, Earth and Planetary Science Letters, 203(1), 507–518, doi:10.1016/S0012-821X(02)00837-3, 2002.

Stebich, M., Rehfeld, K., Schlütz, F., Tarasov, P. E., Liu, J. and Mingram, J.: Holocene vegetation and climate dynamics of NE China based on the pollen record from Sihailongwan Maar Lake, Quaternary Science Reviews, 124, 275–289, doi:https://doi.org/10.1016/j.quascirev.2015.07.021, 2015.

Stein, R., Fahl, K., Schreck, M., Knorr, G., Niessen, F., Forwick, M., Gebhardt, C., Jensen, L., Kaminski, M., Kopf, A., Matthiessen, J., Jokat, W. and Lohmann, G.: Evidence for ice-free summers in the late Miocene central Arctic Ocean, Nature Communications, 7, 11148, doi:10.1038/ncomms11148, 2016.

Stepanek, C. and Lohmann, G.: Modelling mid-Pliocene climate with COSMOS, Geosci. Model Dev., 5, 1221–1243, doi:Stepanek, C. ORCID: https://orcid.org/0000-0002-3912-6271 <https://orcid.org/0000-0002-3912-6271> and Lohmann, G. ORCID: https://orcid.org/0000-0003-2089-733X <https://orcid.org/0000-0003-2089-733X> (2012) Modelling mid-Pliocene climate with COSMOS , Geosci. Model Dev., 5 , pp. 1221-1243 . doi:https://doi.org/10.5194/gmd-5-1221-2012 <https://doi.org/10.5194/gmd-5-1221-2012> , hdl:10013/epic.39137, 2012.

Sun, Y., Wang, X., Liu, Q. and Clemens, S. C.: Impacts of post-depositional processes on rapid monsoon signals recorded by the last glacial loess deposits of northern China, Earth and Planetary Science Letters, 289(1–2), 171–179, doi:10.1016/j.epsl.2009.10.038, 2010.

Svensson, A., Andersen, K. K., Bigler, M., Clausen, H. B., Dahl-Jensen, D., Davies, S. M., Johnsen, S. J., Muscheler, R., Parrenin, F., Rasmussen, S. O., Röthlisberger, R., Seierstad, I., Steffensen, J. P. and Vinther, B. M.: A 60 000 year Greenland stratigraphic ice core chronology, Clim. Past, 12, 2008.

Ünal-İmer, E., Shulmeister, J., Zhao, J.-X., Tonguç Uysal, I., Feng, Y.-X., Duc Nguyen, A. and Yüce, G.: An 80 kyr-long continuous speleothem record from Dim Cave, SW Turkey with paleoclimatic implications for the Eastern Mediterranean, Scientific Reports, 5(1), doi:10.1038/srep13560, 2015.

Wagner, J. D. M., Cole, J. E., Beck, J. W., Patchett, P. J., Henderson, G. M. and Barnett, H. R.: Moisture variability in the southwestern United States linked to abrupt glacial climate change, Nature Geoscience, 3(2), 110–113, doi:10.1038/ngeo707, 2010.

Wainer, K., Genty, D., Blamart, D., Hoffmann, D. and Couchoud, I.: A new stage 3 millennial climatic variability record from a SW France speleothem, Palaeogeography, Palaeoclimatology, Palaeoecology, 271(1–2), 130–139, doi:10.1016/j.palaeo.2008.10.009, 2009.

WAIS Divide Project Members, Buizert, C., Adrian, B., Ahn, J., Albert, M., Alley, R. B., Baggenstos, D., Bauska, T. K., Bay, R. C., Bencivengo, B. B., Bentley, C. R., Brook, E. J., Chellman, N. J., Clow, G. D., Cole-Dai, J., Conway, H., Cravens, E., Cuffey, K. M., Dunbar, N. W., Edwards, J. S., Fegyveresi, J. M., Ferris, D. G., Fitzpatrick, J. J., Fudge, T. J., Gibson, C. J., Gkinis, V., Goetz, J. J., Gregory, S., Hargreaves, G. M., Iverson, N., Johnson, J. A., Jones, T. R., Kalk, M. L., Kippenhan, M. J., Koffman, B. G., Kreutz, K., Kuhl, T. W., Lebar, D. A., Lee, J. E., Marcott, S. A., Markle, B. R., Maselli, O. J., McConnell, J. R., McGwire, K. C., Mitchell, L. E., Mortensen, N. B., Neff, P. D., Nishiizumi, K., Nunn, R. M., Orsi, A. J., Pasteris, D. R., Pedro, J. B., Pettit, E. C., Buford Price, P., Priscu, J. C., Rhodes, R. H., Rosen, J. L., Schauer, A. J., Schoenemann, S. W., Sendelbach, P. J., Severinghaus, J. P., Shturmakov, A. J., Sigl, M., Slawny, K. R., Souney, J. M., Sowers, T. A., Spencer, M. K., Steig, E. J., Taylor, K. C., Twickler, M. S., Vaughn, B. H., Voigt, D. E., Waddington, E. D., Welten, K. C., Wendricks, A. W., White, J. W. C., Winstrup, M., Wong, G. J. and Woodruff,

T. E.: Precise interpolar phasing of abrupt climate change during the last ice age, Nature, 520(7549), 661–665, doi:10.1038/nature14401, 2015.

Wang, Y. J., Cheng, H., Edwards, R. L., An, Z. S., Wu, J. Y., Shen, C.-C. and Dorale, J. A.: A High-Resolution Absolute-Dated Late Pleistocene Monsoon Record from Hulu Cave, China, Science, 294(5550), 2345, doi:10.1126/science.1064618, 2001.

Wassenburg, J. A., Immenhauser, A., Richter, D. K., Jochum, K. P., Fietzke, J., Deininger, M., Goos, M., Scholz, D. and Sabaoui, A.: Climate and cave control on Pleistocene/Holocene calcite-to-aragonite transitions in speleothems from Morocco: Elemental and isotopic evidence, Geochimica et Cosmochimica Acta, 92, 23–47, doi:10.1016/j.gca.2012.06.002, 2012.

Weber, M., Scholz, D., Schroeder-Ritzrau, A., Deininger, M., Spoetl, C., Lugli, F., Mertz-Kraus, R., Jochum, K. P., Fohlmeister, J., Stumpf, C. F. and Riechelmann, D. F. C.: Evidence of warm and humid interstadials in central Europe during early MIS 3 revealed by a multi-proxy speleothem record, Quat. Sci. Rev., 200, 276–286, doi:10.1016/j.quascirev.2018.09.045, 2018.

Wegner, A., Fischer, H., Delmonte, B., Petit, J.-R., Erhardt, T., Ruth, U., Svensson, A., Vinther, B. and Miller, H.: The role of seasonality of mineral dust concentration and size on glacial/interglacial dust changes in the EPICA Dronning Maud Land ice core: EPICA DML DUST RECORD, Journal of Geophysical Research: Atmospheres, 120(19), 9916–9931, doi:10.1002/2015JD023608, 2015.

Wei, W. and Lohmann, G.: Simulated Atlantic Multidecadal Oscillation during the Holocene, J. Climate, 25(20), 6989–7002, doi:10.1175/JCLI-D-11-00667.1, 2012.

Wessel, P. and Smith, W. H. F.: Free software helps map and display data, Eos, Transactions American Geophysical Union, 72(41), 441–446, doi:10.1029/90EO00319, 1991.

Whittaker, T. E., Hendy, C. H. and Hellstrom, J. C.: Abrupt millennial-scale changes in intensity of Southern Hemisphere westerly winds during marine isotope stages 2–4, Geology, 39(5), 455–458, doi:10.1130/G31827.1, 2011.

Williams, P. W.: A 230 ka record of glacial and interglacial events from Aurora Cave, Fiordland, New Zealand, New Zealand Journal of Geology and Geophysics, 39(2), 225–241, doi:10.1080/00288306.1996.9514707, 1996.

Williams, P. W., King, D. N. T., Zhao, J.-X. and Collerson, K. D.: Late Pleistocene to Holocene composite speleothem 18O and 13C chronologies from South Island, New Zealand—did a global Younger Dryas really exist?, Earth and Planetary Science Letters, 230(3–4), 301–317, doi:10.1016/j.epsl.2004.10.024, 2005.

Xiao, J., Porter, S. C., An, Z., Kumai, H. and Yoshikawa, S.: Grain Size of Quartz as an Indicator of Winter Monsoon Strength on the Loess Plateau of Central China during the Last 130,000 Yr, Quaternary Research, 43(1), 22–29, doi:10.1006/qres.1995.1003, 1995.

Xiao, M., Zhang, Q. and Singh, V. P.: Influences of ENSO, NAO, IOD and PDO on seasonal precipitation regimes in the Yangtze River basin, China, International Journal of Climatology, 35(12), 3556–3567, doi:10.1002/joc.4228, 2015.

Yarincik, K. M., Murray, R. W. and Peterson, L. C.: Climatically sensitive eolian and hemipelagic deposition in the Cariaco Basin, Venezuela, over the past 578,000 years: Results from Al/Ti and K/Al, Paleoceanography, 15(2), 210–228, doi:10.1029/1999PA900048, 2000.

Zhang, X., Lohmann, G., Knorr, G. and Xu, X.: Different ocean states and transient characteristics in Last Glacial Maximum simulations and implications for deglaciation, Climate of the Past, 9(5), 2319–2333, doi:10.5194/cp-9-2319-2013, 2013.

Zhou, W., Head, M. J., Lu, X., An, Z., Jull, A. J. T. and Donahue, D.: Teleconnection of climatic events between East Asia and polar, high latitude areas during the last deglaciation, Palaeogeography, Palaeoclimatology, Palaeoecology, 152(1), 163–172, doi:10.1016/S0031-0182(99)00041-3, 1999.